Development of the interfacial microstructure between aluminum nitride and Cu–P–Sn–Ni brazing alloy for different initial titanium layer thicknesses

Nobuyuki Terasaki[a,d*], Aoi Nii[b], Hajime Chiba[b], Touyou Ohashi[a], Kevin M. Knowles[c] , Tohru Sekino[d]

a Innovation Center, Mitsubishi Materials Corporation, Saitama 330-8508, Japan
b Innovation Center, Mitsubishi Materials Corporation, Ibaraki 311-0102, Japan
c Department of Materials Science and Metallurgy, University of Cambridge, 27 Charles Babbage Road, Cambridge, CB3 0FS, UK
d SANKEN (The Institute of Scientific and Industrial Research), Osaka University, 8-1 Mihogaoka, Ibaraki, Osaka 567-0047, Japan

* Corresponding author
E-mail address: terasaki@mmc.co.jp

Abstract

Interfacial microstructures produced between Cu and AlN using a Cu-rich Cu–P–Sn–Ni brazing filler metal as an Ag-free material and a Ti layer as an active metal have been examined. Cu was bonded onto AlN substrates in vacuum for 1 hr at temperatures between 650 °C and 950 °C with 1 and 5 μm thick Ti layers. In contrast to bonding with a 0.5 μm thick Ti layer, four different phases containing Ti and O/N were identified during the development of the Cu/AlN interfacial reaction layer: an amorphous P–Ti–O phase, an amorphous Ti–O phase, a rock-salt titanium oxynitride TiO_xN_y and TiN. The increase in the N concentration in the Ti oxide phase was caused by AlN erosion of the Ti oxide phase in the solid phase promoting the growth of the TiO_xN_y phase when using the 1 μm thick Ti film. In contrast to this, the remelting of the Cu phase at high temperature when in contact with AlN using the 5 μm thick Ti foil promotes the substitution reaction between Ti and AlN, as in the active metal bonding method using Ag.

Introduction

To help meet the long-term temperature goal of the Paris Agreement to mitigate the effects of global warming, many countries have been accelerating their efforts to achieve a carbon-free society. Developing the necessary technology to enable countries to bring about the social changes required within society has meant that the replacement of conventional power modules equipped with Si–IGBT (silicon–insulated gate bipolar transistor) chips by those equipped with SiC–MOSFET (silicon carbide–metal-oxide-semiconductor field-effect transistor) chips, which have both high-voltage and low-resistance, is progressing rapidly for industrial applications [1–5]. An insulating substrate for a power module is composed of a high thermal conductivity metal layer such as aluminum (Al) or copper (Cu), and a ceramic insulating layer such as aluminum nitride (AlN), silicon nitride (Si_3N_4) or aluminum oxide (Al_2O_3). These metal-bonded ceramic substrates are grouped into one type of aluminum circuit substrate: direct bonding aluminum (DBA) substrates [1, 6, 7], and two types of copper circuit substrates: direct bonding copper (DBC) substrates [8, 9] and active metal bonding (AMB) substrates [10, 11].

The AMB method is a general one for achieving good bonding between metals and ceramics in a vacuum atmosphere: an active metal compound layer containing a ceramic component such as C, N and O is formed by an interfacial reaction on the surface of the ceramic during the active metal brazing [10–15]. To overcome problems with using Ag–Cu-based alloys with Ti as the active metal in power modules, an Ag-free Cu-rich active metal braze composition has recently been developed by combining the Cu–P based eutectic system with Ti as the active metal. This has been shown to produce strong interfacial bonds between Cu and both AlN and Si_3N_4 [16–20].

With this Cu-rich braze alloy the chemical reactions which arise at the Cu/AlN interface are determined by the bonding temperature. When a 0.5 μm thick Ti film is used together with a 25 μm thick foil of this Cu-rich braze as the bonding media, the Cu/AlN interfacial microstructure changes from an amorphous P–Ti–O phase at 650 °C into an amorphous Ti–O phase at 750 °C, and then a rutile TiO_2 phase at 850 °C or higher bonding temperatures [20]. The oxygen in this system comes from the thin native surface oxide layers on the various materials being bonded, such as those on the AlN and the brazing

foil. The Cu/AlN interfacial structure where the rutile TiO_2 phase is dominant contributes significantly to the improvement of the Cu/AlN interfacial strength [20]. The thickness of the Ti–O based phase observed at the Cu/AlN interface in this recent study of ours is at most 10 nm [20]. This is extremely thin compared to the initial 0.5 μm Ti film thickness. This 10 nm thickness contrasts with the 20 μm thick TiN layer reported by Nakao et. al. [21] formed at Cu/AlN interfaces after a heat treatment of 900 °C for 0.5 hr when using a 0.3–0.4 mm thick Cu–22 wt%Ti eutectic brazing foil [22]. The effective initial thickness of Ti in this Ag-free Cu–22 wt%Ti eutectic brazing foil was 110–140 μm. These observations suggest that the combination of Ag-free material and Ti is not necessarily sufficient to promote the formation of a Ti–O based phase at the Cu/AlN interface. Therefore, in the work reported here, we have examined the effect of increasing the Ti layer thickness on the Cu/AlN interfacial microstructure when fabricated by the Ag-free AMB method. Particular attention has been paid to the nature of the Ti compound phase types formed at these Cu/AlN interfaces as a function of bonding temperature.

Experimental method

An amorphous brazing alloy Cu–6.3 wt%P–9.3 wt%Sn–7 wt%Ni with a thickness of 25 μm, as used in our recent work, was used as the Ag-free material for bonding between Cu and AlN substrates [20]. The solidus and liquidus temperatures of this Cu–rich alloy are 600 °C and 630 °C, respectively [20]. In this new work, two thicker Ti layers of 1 and 5 μm were prepared. For the thinner of these two layers, a 1 μm thick film was deposited by physical vapour deposition on one side of 300 μm thick oxygen free copper (OFC). For the thicker of these two layers, a 5 μm thick TPC270C Ti foil was used. According to Japan Industrial Standards (JIS), TPC270C foil has the highest purity of all commercially available pure Ti. It is notable for its softness and excellent workability. AlN polycrystalline substrates with 1 mm thickness commonly used for power module applications were selected. The substrates all contained yttria (Y_2O_3) as a sintering additive.

These materials were all cut into 5 mm × 10 mm rectangular pieces and were then stacked in the order: Cu, Ti deposited film or Ti foil, Cu–P–Sn–Ni brazing foil and AlN substrate. The stacked samples were brazed in vacuum at 650, 750, 850 and 950 °C for 1 hr under 1 MPa pressure with heating and

cooling rates of 10 °C/min.

Cross-sections of the resulting joints were observed by electron probe micro analysis (EPMA), scanning electron microscopy (SEM), and scanning transmission electron microscopy (STEM) equipped with energy dispersive X–ray spectroscopy (EDS). Metallography samples for SEM and EPMA mounted in an acrylic polymer at room temperature were polished using conventional metallographic techniques. In addition, the final polishing for these samples was performed using an argon-based ion beam polisher (ArBlade 5000, Hitachi High-Tech) to obtain the final flat cross-sections before being coated with a thin carbon layer. The microstructures and elemental distributions of all samples were analyzed using a EPMA apparatus (JXA–8530F, JEOL) operated at 15 kV. The thickness of the Cu/AlN thin sections for STEM analysis, prepared using a focused ion beam (FIB) instrument (Scios, Thermo Fisher Scientific), ranged from 30 to 100 nm. Elemental distributions of the thin sections were evaluated on a STEM (Titan G2 ChemiSTEM, Thermo Fisher Scientific) equipped with an EDS system (NSS7, Thermo Fisher Scientific) operated at 200 kV.

Results and discussion

Cross-sectional backscattered electron (BSE) images of the Cu/AlN interfaces bonded at 650 °C for 1 hr are shown in Fig. 1(a) and 1(b), for the initial 1 and 5 μm thick Ti layers, respectively. At this temperature just above the liquidus temperature of the Cu–P–Sn–Ni brazing foil, the Cu/AlN interface appears to fit the surface shape of the polycrystalline AlN substrate well with no gaps and/or pores. This suggests that the Cu–P–Sn–Ni liquidus phase has good wettability to the AlN substrate through the presence of the initial Ti active metal. In both Fig. 1(a) and 1(b), the Cu layer is divided into two regions by the Ti-containing layer formed ≈8 μm away from the surface of the AlN substrate.

The reaction between the Cu–P–Sn–Ni brazing foil and the 1 μm thick Ti film consumes the entire Ti film. The product in this reaction is mainly Ti_5P_3 (hexagonal, $P6_3/mcm$, a = 7.234 Å, c = 5.090 Å) [23, 24], which is formed as a continuous layer. In contrast to this observation with the 1 μm thick Ti film, there is still unreacted Ti foil after the chemical reaction between the Cu–P–Sn–Ni brazing foil and the 5 μm thick Ti foil, as shown in Fig. 1(b). It is

convenient to term this unreacted Ti foil a residual Ti layer.

The cross-sectional structure between this residual Ti layer and the AlN substrate is composed of the following compounds in order from the residual Ti layer side: $Cu_{0.9}TiNi_{1.1}$(tetragonal, $I4/mmm$, a = 3.12 Å, c = 7.965 Å) [25], TiP (hexagonal, $P6_3/mmc$, a = 3.499 Å, c = 11.700 Å) [24, 26, 27], Ti_5P_3 [23, 24] and Cu (cubic, $Fm\bar{3}m$, a = 3.615 Å). The brightness of the BSE image also increases gradually from the residual Ti layer toward the Cu surface. This suggests that multiple Cu–Ti intermetallic compounds (IMCs) with different composition ratios such as Cu_4Ti (orthorhombic, $Pnma$, a = 4.525 Å, b = 4.341 Å, c = 12.953 Å) [22, 28, 29], Cu_4Ti_3 (tetragonal, $I4/mmm$, a = 3.126 Å, c = 19.964 Å) [27, 28], CuTi (tetragonal, $P4/nmm$, a = 3.107 Å, c = 5.919 Å) [28, 29] and $CuTi_2$ (tetragonal, $I4/mmm$, a = 2.944 Å, c = 10.786 Å) [28, 29] are formed in layers by solid-phase diffusion bonding between the Cu layer and the Ti foil. In addition, it can be seen that a number of voids are distributed in the Cu–Ti IMCs, as shown in Fig. 1(b). This suggests that the oxide films present on the surface of the Cu plate and Ti foil inhibit the interdiffusion between Cu and Ti.

Cross-sectional BSE images together with elemental distributions of the Cu/AlN interface bonded at 650 °C are shown in Figs. 2 and 3, for the initial 1 and 5 μm thick Ti layers, respectively. The grey area in the AlN layer shown in Fig. 3(a) is yttria, a sintering additive in the AlN substrate. Sn diffuses beyond the P-containing IMCs layer towards the Cu surface side when using the 1 μm thick Ti layer, as is evident from Fig. 2(c). By contrast, the Sn is localized between the P-containing layer and the AlN substrate when using the 5 μm Ti layer, as can be seen in Fig. 3(c).

It is suggested that the difference in Sn distribution is caused by a difference in the degree of dissolution of the TiN layer into the Cu–P–Sn–Ni liquid phase. P-containing IMC particles are precipitated by the reaction between Ti and P when dissolving the entire 1 μm thick Ti layer in the Cu–P–Sn–Ni liquid phase, forming a layered structure. Consumption of P, the melting-point lowering element that makes up the Cu–P–Sn–Ni brazing foil, promotes solidification from the P-containing IMCs layer side to the AlN side. The Sn which concentrated at the Cu/AlN interface during the isothermal solidification process eventually diffuses into Cu toward the Cu surface side. This same solidification process is expected to occur when using the 5 μm thick Ti layer. However, the formation of the residual Ti layer present in Fig.

1(b) and Fig. 3(a) would suggest that not all of the Ti layer is dissolved into the Cu–P–Sn–Ni liquid phase. In addition, the diffusion length of Sn into Ti is only ≈1 nm after 1 h at 650 °C [30]. Hence, the residual Ti layer functions as a diffusion inhibition layer and suppresses the diffusion of Sn toward the Cu surface side. In addition, it can be seen from Figs. 2(a)–(c) and 3(a)–(c) that there is no precipitation of either Cu_3Sn (orthorhombic, *Cmcm*, $a = 5.529$ Å, $b = 47.75$ Å, $c = 4.323$ Å) or Cu_6Sn_5 (monoclinic, $C2/c$, $a = 11.022$ Å, $b = 7.282$ Å, $c = 9.827$ Å, $\beta = 98.84°$) in the regions where Cu and Sn coexist [31–33]. This supports the formation of a dense Cu layer without Kirkendall void generation [34, 35] at the Cu/AlN interface.

Cross-sectional BSE images and TEM images of a Cu/AlN interface, together with nano-beam electron diffraction (NBD) patterns of a Cu/AlN interfacial reaction layer after bonding for 1 hr between 650 °C and 950 °C with the 1 μm thick Ti layer are shown in Fig. 4. The grey area in the AlN layer shown in BSE images of Fig. 4 is yttria. The NBD patterns were acquired from the areas circled in yellow in the corresponding TEM images. It can be seen from the BSE images that the Ti-containing layer composed of TiP and Ti_5P_3 is formed at a distance of ≈8 μm from the surface of the AlN substrate at all these heating temperatures. Within this range of bonding temperatures, the morphology of these Ti-containing layers is in essence independent of the bonding temperature. P is the main melting point lowering element of the Cu–P–Sn–Ni brazing alloy. This therefore suggests that its consumption through intermetallic compound formation reaction with Ti causes the Cu–P–Sn–Ni liquid phase to solidify in the early stages of the heating process. This means that the interfacial reaction between Cu and AlN when using the 1 μm thick Ti film proceeds mainly in the solid phase.

Furthermore, it can be seen from the NBD patterns in Fig. 4 that the Cu/AlN interfacial reaction layers are composed of an amorphous phase at 750 °C or lower, and a crystalline phase at 850 °C or higher. The thicknesses of these crystalline phases are ≈7 nm at 850 °C and ≈35 nm at 950 °C, respectively. EDS line profiles after bonding for 1 hr at (a) 850 °C and (b) 950 °C with this initial 1 μm thick Ti film are shown in Fig. 5. The EDS line profiles were acquired from the lines defined by the yellow arrows shown in the corresponding TEM images in Figs. 4(c) and 4(d), respectively. The high Ti concentration at the Cu/AlN interfacial reaction layer is clear, with signals of O and N overlapping with Ti. This suggests that the crystalline Cu/AlN

interfacial reaction layer consists of O-containing TiN phase, given the NBD patterns shown in Fig 4. These NBD patterns can be indexed in terms of TiN. TiN has the rock-salt crystal structure and occurs over a wide range of stoichiometry within the Ti–N system. Substitution of oxygen for nitrogen within this phase can also occur to give an extensive phase field within the ternary Ti–O–N system in which rock-salt titanium oxynitrides of the general composition TiO_xN_y occur [36–40].

Cross-sectional BSE images and TEM images of a Cu/AlN interface, together with NBD patterns of a Cu/AlN interfacial reaction layer after bonding for 1 hr between 650 °C and 950 °C with the 5 μm thick Ti layer are shown in Fig. 6. The grey area in the AlN layer shown in BSE images of Figs. 6(b) and 6(d) is yttria. The NBD patterns were acquired from the areas circled in yellow in the corresponding TEM images. It can be seen that as the heating temperature rises from 650 °C to 750 °C the residual Ti layer disappears because of the growth of the layer of Cu–Ti IMCs. In addition, it can be seen that the layer of Cu–Ti IMCs disappears and an obvious interfacial reaction layer is formed at the AlN interface at 850 °C or higher. The thickness of these interfacial reaction layers, which are seen to be crystalline TiN phase from the NBD patterns shown in Fig. 6, are ≈0.5 μm at 850 °C and ≈1 μm at 950 °C, respectively.

The Cu/AlN interfacial reaction layers are composed of an amorphous phase at a heating temperature of 750 °C or lower when using 5 μm thick Ti foil. This is the same as with the Cu/AlN interfacial structure when using an initial 1 μm thick Ti foil, as shown in Fig. 4. Cross-sectional high angle annular dark field (HAADF) images together with elemental distributions of the Cu/AlN interface bonded at 650 °C and 750 °C for 1 hr with initial 5 μm Ti layers are shown in Figs. 7 and 8, respectively. Both Sn and Ni omitted from these elemental maps are in solid solution within Cu near the Cu/AlN interface. The highest signals in the P, Ti and O maps are positioned at the Cu/AlN interface, as can be seen in Fig. 7(c)–(e). By comparison, only Ti and O signals are uniformly distributed at the Cu/ AlN interfacial reaction layer, whereas P is enriched at the interface between Cu and interfacial reaction layer, as shown in Fig. 8(c)–(e), despite the base signal of P in the Cu in Fig. 8(c) being relatively high.

The transformation in the Cu/AlN interfacial reaction layer with increasing heating temperature from 650 °C to 750 °C for the 5 μm thick Ti

foil shown in Figs. 7 and 8 is similar to the transformation observed for an initial 0.5 μm thick Ti film [20]. This suggests that at 650 °C and 750 °C the reaction between Cu and AlN does not depend on the thickness of the initial Ti layer. Furthermore, it can be seen that the thickness of these Ti–O based phases observed at the Cu/AlN interface under these bonding conditions is at most 10 nm for 0.5 – 5 μm thick Ti material, which is independent of whether the source of the Ti material is a film or a foil. This suggests that the oxygen component of the Ti–O based phases is derived mainly from the surface oxide layer of the AlN and the brazing material, rather than from any oxygen from the surface and grain boundaries of the Ti material.

Quantitative analysis using EPMA of the Cu phase 4 μm away from a Cu/AlN bonding interface after bonding for 1 hr at 650 °C and 750 °C is shown in Table 1. The Sn concentration decreases by half between 650 °C and 750 °C using the 1 μm thick Ti film, while there is only a 5 % decrease using the 5 μm thick Ti foil. This is consistent with the Ti residual layer and/or the thick Cu–Ti IMCs layer strongly inhibiting the diffusion of Sn into the Cu surface side. This Sn concentration, which is relatively insensitive to the 100 °C temperature rise for the 5 μm thick Ti foil, is larger than the solid solubility of Sn in Cu at 850 °C (5.6 at%) [31–33]. This implies that the Cu–Sn liquid phase generated by the remelting of the Cu phase in contact with the AlN substrate melts the layer of Cu–Ti IMCs above 850 °C. This means that the Ti-containing liquid phase generated at a relatively high heating temperature helps to promote the substitution reaction between Ti and AlN on the surface of the AlN substrate, in a manner similar to the AMB method using Ag.

A simple schematic of the Cu/AlN interfacial structure bonded for 1 hr at between 650 °C and 950 °C as a function of bonding temperature and thickness of the initial Ti layer is shown in Fig. 9. When using a 0.5 μm thick Ti film, the rutile TiO_2 phase grows locally in the Cu/AlN interfacial structure at 750 °C because of partial crystallization of an amorphous Ti–O phase which is dominant [20]. The Cu/AlN interfacial structure transforms from the amorphous P–Ti–O phase to the amorphous Ti–O phase independently of the Ti layer thickness at 750 °C or lower. Above 750 °C, the interfacial reaction phase formed at the Cu/AlN interface depends on the thickness of the Ti layer, i.e., rutile TiO_2 for a 0.5 μm thick Ti film, TiO_xN_y for a 1 μm thick Ti film and TiN for a 5 μm thick Ti foil. Ti concentrations in the amorphous P–Ti–O phase and the amorphous Ti–O phase as a function of the initial Ti material in the

range of thickness 0.5 – 5 μm are shown in Fig. 10.

The Ti concentration in the amorphous Ti–O phase increases as the Ti layer thickness increases, whereas, within experimental error, the Ti concentration of the amorphous P–Ti–O phase is independent of the initial thickness of the Ti material. The highest Ti concentration achieved of 43.0 at%. is in the amorphous Ti–O phase at 750 °C when using a 5 μm thick Ti foil. In addition, from our previous work [20], the N concentration in the rutile TiO_2 phase increases from 6.2 at% to 10.7 at% with increasing heating temperature from 850 °C to 950 °C when using a 0.5 μm thick Ti film. This implies that the difference in Cu/AlN interfacial reaction layer between the initial 0.5 μm and 1 μm thick Ti film is caused by the difference in the amount of erosion of the AlN substrate through the Ti concentration in the amorphous (P–)Ti–O phase. Hence, an increase in the N concentration at the Cu/AlN interface promotes the formation of TiO_xN_y, rather than TiO_2, as the crystallization product of the amorphous Ti–O phase. This growth process of the TiO_xN_y phase for a 1 μm thick Ti film is completely different from the formation process of the TiN phase, which is similar to the process in the Ag–Cu–Ti based system, as a consequence of the melting of the Cu phase for the 5 μm thick Ti foil.

Conclusions

The effect of increasing the Ti layer thickness on the development of the Cu/AlN interfacial microstructure when using a Cu-rich Cu–P–Sn–Ni brazing filler metal as an Ag-free material has been studied using a variety of electron microscope-based techniques. With both the initial 1 μm and 5 μm Ti layers, amorphous P–Ti–O phase at 650 °C and amorphous Ti–O phase at 750 °C were formed at the Cu/AlN interface, respectively. At both these bonding temperatures, P was concentrated at the Cu/amorphous Ti–O phase interface. These transformations in the Cu/AlN interfacial structure were similar to those reported when using a 0.5 μm thick Ti film [20]. The Cu/AlN interfacial reaction layers at 850 °C or higher were composed of TiN-based phases. The increase in N concentration in the Ti oxide phase due to the erosion of the amorphous Ti–O phase and/or the rutile TiO_2 phase into AlN promotes the formation through solid state chemical reaction of a rock-salt titanium oxynitride of the general composition TiO_xN_y phase when using a 1 μm thick Ti film. When using the 5 μm thick Ti foil, the Cu–Sn liquid phase derived

from the remelting of the Cu phase in contact with AlN promoted the substitution reaction between Ti and AlN, which is similar to the Cu/AlN interfacial reaction process using an Ag–Cu–Ti active metal braze.

Author contributions

The manuscript was written through contributions of all authors. All authors have given approval to the final version of the manuscript.

Declarations

Conflict of interest: the authors declare that they have no conflict of interest.

References

[1] M. Toriumi, H. Tanaka, H. Yoshida, The development of Al circuit substrate for power module, IMC 1994 Proceedings, 1994, 104–109.

[2] C.-K. Kim, V.K. Sood, G.-S. Jang, S.-J. Lim, S.-J. Lee, HVDC Transmission: Power Conversion Applications in Power Systems, John Wiley & Sons Ltd., New York, 2009.

[3] M. Furuhashi, S. Tomohisa, T. Kuroiwa, S. Yamakawa, Practical applications of SiC–MOSFETs and further developments, Semiconductor Science and Technology, 31(3), 2016, 034003.

[4] L. Stevanovic, B. Rowden, M. Harfman-Todorovic, P. Losee, A. Bolotnikov, S. Kennerly, T. Schuetz, F. Carastro, R. Datta, F. Tao, R. Raju, P. Cioffi, High performance SiC MOSFET module for industrial applications, Proceedings of the 28th International Symposium on Power Semiconductor Devices and ICs, 2016, 479–482.

[5] M. Piton, B. Chauchat, J.F. Servière, Implementation of direct chip junction temperature measurement in high power IGBT module in operation - railway traction converter, Microelectronics Reliability, 88–90, 2018, 1305–1310.

[6] X.S. Ning, Y. Ogawa, K. Suganuma., Interface of aluminum/ceramic power substrates manufactured by casting-bonding process, Materials Research Society Symposium Proceedings, 445, 1996, 101–106.

[7] Y. Kuromitsu, Y. Nagatomo, K. Akiyama, N. Shibata, Y. Ikuhara, Direct-bonded aluminum on aluminum nitride substrates by transient liquid phase bonding, Journal of the Ceramic Society of Japan, 125(3), 2017, 165–167.

[8] J.F. Burgess, C.A. Neugebauer, G. Flanagan, R.E. Moore, The direct bonding of metals to ceramics and application in electronics, Electrocomponent Science and Technology, 2, 1976, 233–240.
[9] J. Schulz-Harder, Advantages and new development of direct bonded copper substrates, Microelectronics Reliability, 43(3), 2003, 359–365.
[10] N.Yu. Taranets, H. Jones, Wettability of aluminum nitride based ceramics of different porosity by two active silver based brazing alloys, Materials Science and Engineering A, 379, 2004, 251–257.
[11] N. Terasaki, T. Ohashi, Y. Nagatomo, Y. Kuromitsu, A.A. Shirzadi, A new method for liquid-phase bonding of copper plates to aluminum nitride (AlN) substrates used in high-power modules, Journal of Materials Science: Materials in Electronics, 30, 2019, 6552–6555.
[12] O. Saitoh, A. Suzumura, H. Ogawa, The corrosion phenomena of ruby by active metal brazing filler (Ag–Cu–Ti) at the brazing interface, Quarterly Journal of the Japan Welding Society, 14(4), 1996, 717–722.
[13] M. Ali, K.M. Knowles, P.M. Mallinson, J.A. Fernie, Interfacial reactions between sapphire and Ag–Cu–Ti-based active brazed alloys, Acta Materialia, 103, 2016, 859–869.
[14] S. Kato, T. Yano, T. Iseki, Interfacial structures between Ag–Cu–Ti alloys and sintered SiC with various additives, Journal of the Ceramic Society of Japan, 101(3), 1993, 325–330.
[15] F.-L. Sun, J.-C. Feng, D. Li, Bonding of CVD diamond thick films using an Ag–Cu–Ti brazing alloy, Journal of Materials Processing Technology, 115(3), 2001, 333–337.
[16] N. Terasaki, Y. Nagatomo, T. Nagase, Y. Kuromitsu, New power module structures consisting of both Cu and Al bonded to AlN substrates with an Al base plate, Proceedings of 8th International Conference on Integrated Power Electronics Systems, 2014, 456–460.
[17] N. Terasaki, Development of a high reliability power-module substrate via new bonding process using Ag-free bonding material, Journal of Smart Processing, 7(5), 2018, 172–175.
[18] N. Terasaki, Development of a high reliability power-module substrate via metal/ceramic bonding technology, in Development and Mounting Technology of Printed Wiring Board Materials, Technical Information Institute Co., Ltd., Tokyo, 2020, 148–155.
[19] S. Takakuwa, N. Terasaki, T. Ohashi, Development of a new bonding

technique between Cu and Si_3N_4 by using Ag-free bonding material, Proceedings of the 26th Symposium on Microjoining and Assembly Technology in Electronics, 26, 2020, 281–284.
[20] N. Terasaki, N. Kon, H. Chiba, T. Ohashi, Y. Nagatomo, Y. Kuromitsu, K.M. Knowles, Interfacial structures between aluminum nitride and Cu–P–Sn–Ni brazing alloy with Ti film, Journal of Materials Science, 56, 2021, 8778–8788.
[21] Y. Nakao, K. Nishimoto, K. Saida, K. Murabe, Y. Fukaya, Microstructure of bonding layer in aluminum nitride to metals joints bonded by active brazing method, Quarterly Journal of the Japan Welding Society, 12(1), 1994, 115–121.
[22] H. Okamoto, Cu–Ti (Copper-Titanium), Journal of Phase Equilibria, 23(6), 2002, 549–550.
[23] G. Brauer, K. Gingerich, M. Knausenberger, Kristallstruktur des Titanphosphids Ti_5P_3, Angewandte Chemie, 76(4), 1964, 187.
[24] H. Okamoto, P–Ti (Phosphorus-Titanium), Journal of Phase Equilibria and Diffusion, 28(6), 2007, 587.
[25] F.J.J.V. Loo, G.F. Bastin, A.J.H. Leenen, Phase relations in the ternary Ti–Ni–Cu system at 800 and 870 °C, Journal of the Less-Common Metals, 57, 1978, 111–121.
[26] N. Schönberg, An X-ray investigation of transition metal phosphides, Acta Chemica Scandinavica, 8(2), 1954, 226–239.
[27] T. Lundström, P.-O. Snell, Studies of the crystal structures and phase relationships in the Ti–P system, Acta Chemica Scandinavica, 21(5), 1967, 1343–1352.
[28] H.-U. Pfeifer, S. Bahn, K. Schubert, Zum Aufbau des Systems Ti–Ni–Cu und einiger quasihomologer Legierungen, J. Less-Common Metals 14(3), 1968, 291–302.
[29] P. Villars, L.D. Calvert, Pearson's Handbook of Crystallographic data for Intermetallic Phases, Volume 2, American Society for Metals, Metals Park, Ohio, 2037–2038.
[30] R.A. Pérez, M. Behar, F. Dyment, Diffusion study of Sn implanted in α-Ti, Philosophical Magazine A, 75, 1997, 993–1004.
[31] N. Saunders, A.P. Miodownik, The Cu–Sn (Copper-Tin) system, Bulletin of Alloy Phase Diagrams, 11(3), 1190, 278–287.
[32] S. Fürtauer, D. Li, D. Cupid, H. Flandorfer, The Cu–Sn phase diagram,

Part I: New experimental results, Intermetallics, 34, 2013, 142–147.
[33] D. Li, P. Franke, S. Fürtauer, D. Cupid, H. Flandorfer, The Cu–Sn phase diagram, Part I: New thermodynamic assessment, Intermetallics, 34, 2013, 148–158.
[34] J. Wang, J. Chen, L. Zhang, Z. Zhang, Y. Han, X. Hu, H. Lu, S. Zhang, Forming mechanism and growth of Kirkendall voids of Sn/Cu joints for electronic packaging: A recent review, Journal of Advanced Joining Processes, 6, 2022, 100125.
[35] B. Wang, W. Li, S. Zhang, X. Liu, K. Pan, Effect of electric current stressing on mechanical performance of solders and solder joints: A review, Journal of Materials Science, 57, 2022, 17533–17562.
[36] C.H. Shin, G. Bugli, G. Djega-Mariadassou, Preparation and characterization of titanium oxynitrides with high specific surface areas, Journal of Solid State Chemistry 95, 1991, 145–155.
[37] H. Yang, P.G. McCormick, Synthesis of titanium oxynitride by mechanical milling, Journal of Materials Science 28, 5663–5667.
[38] G. Hyett, M.A. Green, I.P. Parkin, The use of combinatorial chemical vapor deposition in the synthesis of $Ti_{3-\delta}O_4N$ with $0.06 < \delta < 0.25$: a titanium oxynitride phase isostructural to anosovite, Journal of the American Chemical Society, 129, 2007, 15541–15548.
[39] S.G. Seo, C.-H. Park, H.-Y. Kim, W.H. Nam, M. Jeong, Y.-N. Choi, Y.S. Lim, W.-S. Seo, S.-J. Kim, J.Y. Lee, Y.S. Cho, Preparation and visible-light photocatalysis of hollow rock-salt $TiO_{1-x}N_x$ nanoparticles, Journal of Materials Chemistry A, 1(11), 2013, 3639–3644.
[40] K. Rees, E. Lorusso, S.D. Cosham, A.N. Kulak, G. Hyett, Combining single source chemical vapour deposition precursors to explore the phase space of titanium oxynitride thin films, Dalton Transactions, 47, 2018, 10536–10543.

Figures and Table captions

Fig. 1 Cross-sectional BSE images of a Cu/AlN interface after bonding at 650 ℃ for 1 hr with initial Ti layers (a) 1 μm and (b) 5 μm thick.

Fig. 2 (a) BSE image of a Cu/AlN interface at 650 °C for 1 hr with an initial 1 μm thick Ti film, together with the elemental distribution of (b) Cu, (c) Sn, (d) P, (e) Ni, (f) Ti, (g) Al and (h) N.

Fig. 3 (a) BSE image of a Cu/AlN interface at 650 °C for 1 hr with an initial 5 μm thick Ti foil, together with the elemental distribution of (b) Cu, (c) Sn, (d) P, (e) Ni, (f) Ti, (g) Al and (h) N.

Fig. 4 Cross-sectional BSE and TEM images of a Cu/AlN interface with nano beam electron diffraction patterns of the interfacial reaction layer after bonding for 1 hr with an initial 1 μm thick Ti film at (a) 650 °C, (b) 750 °C, (c) 850 °C and (d) 950 °C. In (c) and (d) the electron diffraction patterns index to TiN, which together with the compositional mapping presented in Fig. 5 is consistent with a rock-salt titanium oxynitride of the more general composition TiO_xN_y. The yellow arrows in the TEM images in Figs. (c) and (d) indicate the positions and directions of the EDS line profiles shown in Fig. 5.

Fig. 5 EDS analyses of a Cu/AlN interfacial reaction layer after bonding for 1 hr with an initial 1 μm thick Ti film at (a) 850 °C and (b) 950 °C. These EDS line profiles were acquired from the lines defined by the yellow arrows shown in the corresponding TEM images in Figs. 4(c) and 4(d), respectively.

Fig. 6 Cross-sectional BSE and TEM images of a Cu/AlN interface with nano beam electron diffraction patterns of the interfacial reaction layer after bonding for 1 hr with an initial 5 μm Ti foil at (a) 650 °C, (b) 750 °C, (c) 850 °C and (d) 950 °C.

Fig. 7 (a) HAADF image of a Cu/AlN interface after bonding at 650 °C for 1 hr with an initial 5 μm Ti foil, together with the elemental distribution of (b) Cu, (c) P, (d) Ti, (e) O, (f) Al and (g) N obtained by EDS.

Fig. 8　(a) HAADF image of a Cu/AlN interface after bonding at 750 °C for 1 hr with an initial 5 μm Ti foil, together with the elemental distribution of (b) Cu, (c) P, (d) Ti, (e) O, (f) Al and (g) N obtained by EDS.

Fig. 9　Cu/AlN interfacial structure classification as a function of temperature and Ti film/foil. thickness.

Fig. 10　Dependence of the Ti concentration in the amorphous phase of a Cu/AlN interface on the initial Ti film/foil thickness after bonding for 1 hr at 650 °C and 750 °C. Within experimental error in the 0.5 – 5 μm thickness range shown, the Ti concentration of the amorphous P–Ti–O phase is independent of the initial thickness of the Ti material, whereas that of the amorphous Ti–O phase increases as the initial thickness of the Ti material increases.

Table 1　Quantitative analysis of a Cu phase 4 μm away from a Cu/AlN bonding interface after bonding for 1 hr at the specified temperatures.

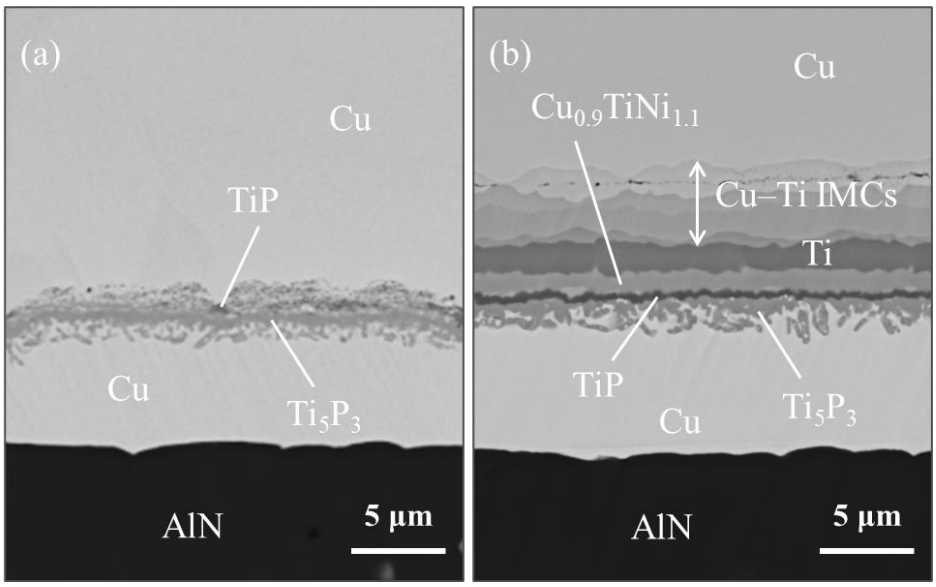

Fig. 1 Cross-sectional BSE images of a Cu/AlN interface after bonding at 650 ℃ for 1 hr with initial Ti layers (a) 1 μm and (b) 5 μm thick.

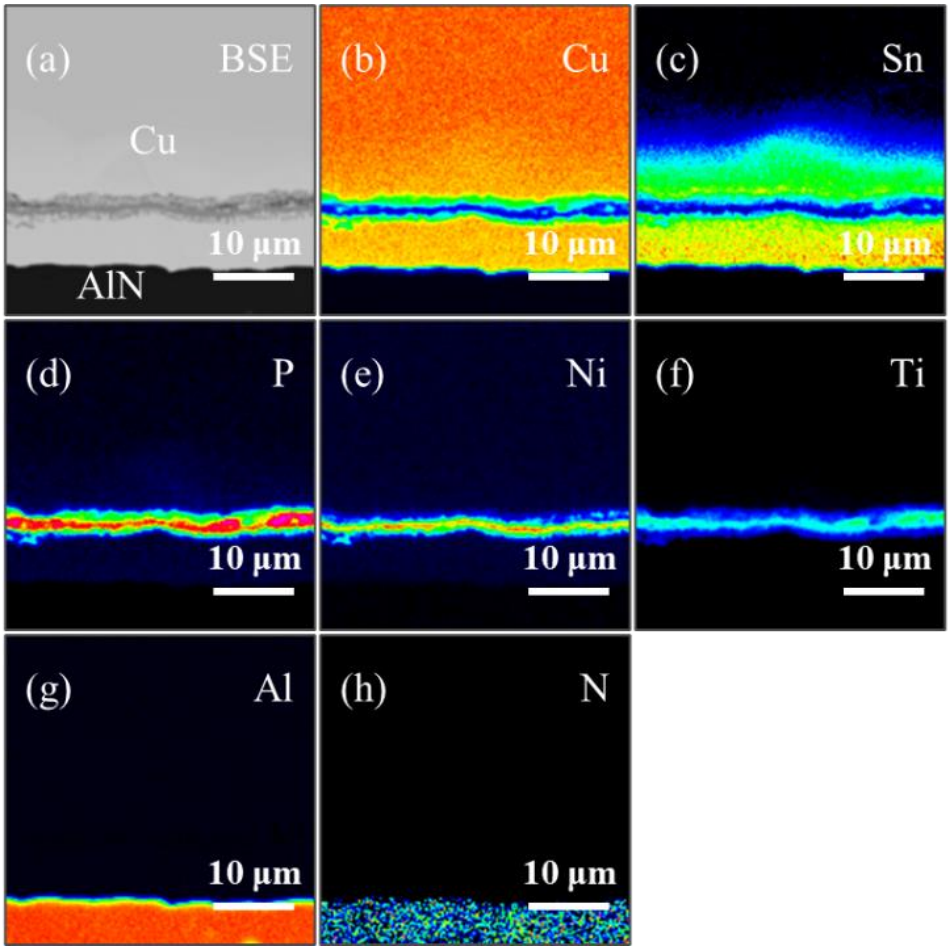

Fig. 2 (a) BSE image of a Cu/AlN interface at 650 °C for 1 hr with an initial 1 μm thick Ti film, together with the elemental distribution of (b) Cu, (c) Sn, (d) P, (e) Ni, (f) Ti, (g) Al and (h) N.

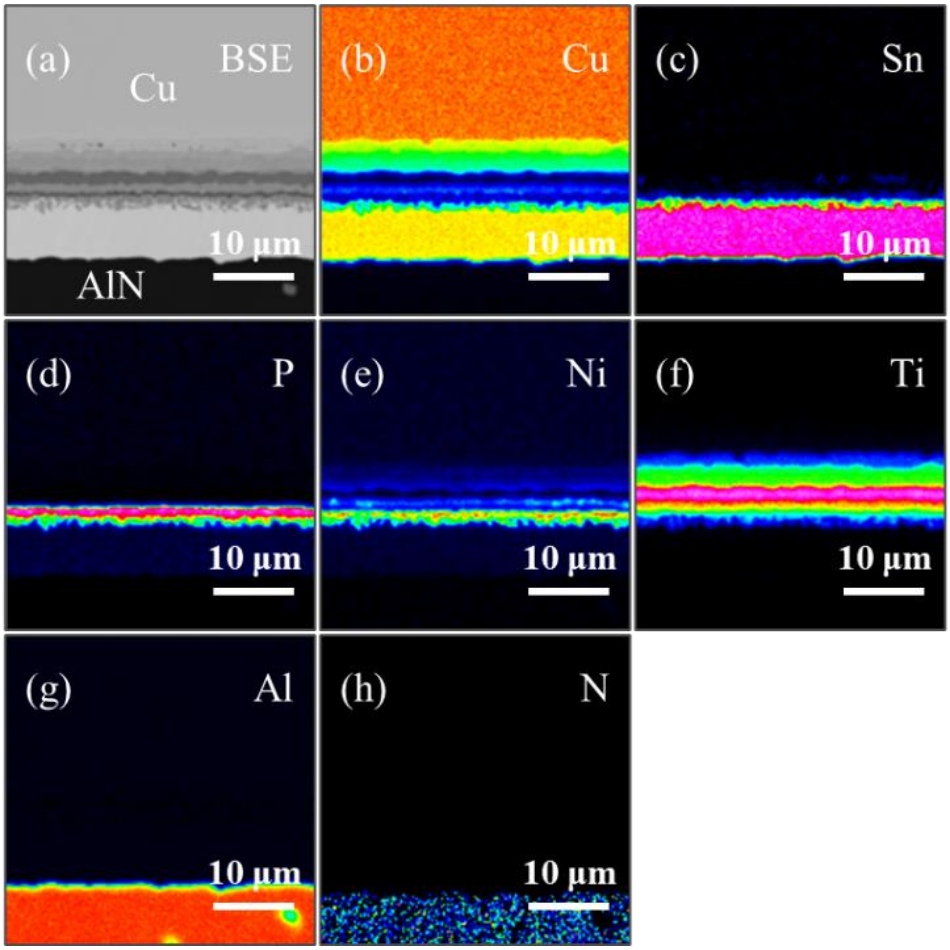

Fig. 3 (a) BSE image of a Cu/AlN interface at 650 °C for 1 hr with an initial 5 μm thick Ti foil, together with elemental distribution of (b) Cu, (c) Sn, (d) P, (e) Ni, (f) Ti, (g) Al and (h) N.

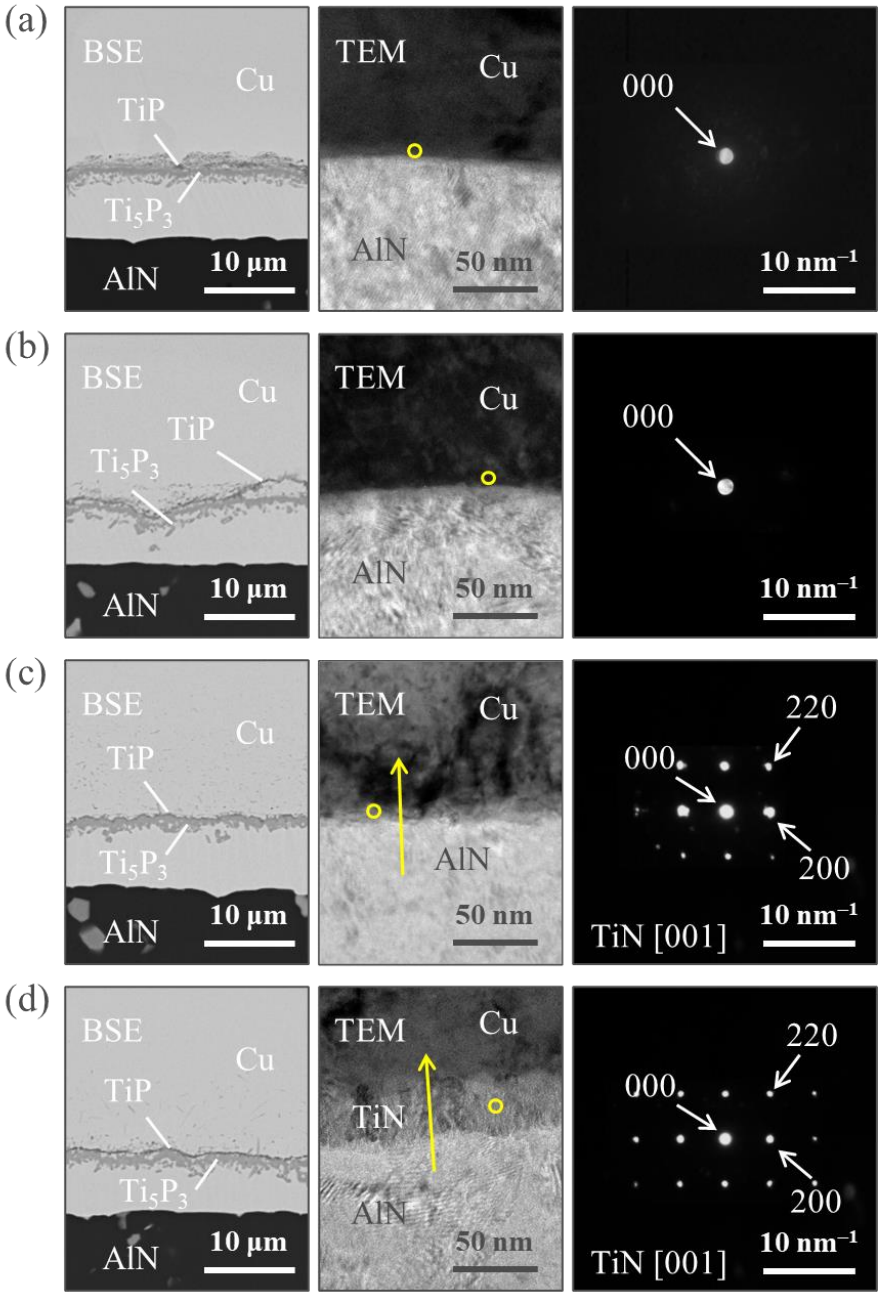

Fig. 4 Cross-sectional BSE and TEM images of a Cu/AlN interface with nano beam electron diffraction of interfacial reaction layer after bonding for 1 hr with an initial 1 μm thick Ti film at (a) 650 °C, (b) 750 °C, (c) 850 °C and (d) 950 °C. In (c) and (d) the electron diffraction patterns index to TiN, which together with the compositional mapping presented in Fig. 5 is consistent with a rock-salt titanium oxynitride of the more general composition TiO_xN_y. The yellow arrows in the TEM images in Figs. (c) and (d) indicate the positions and directions of the EDS line profiles shown in Fig. 5.

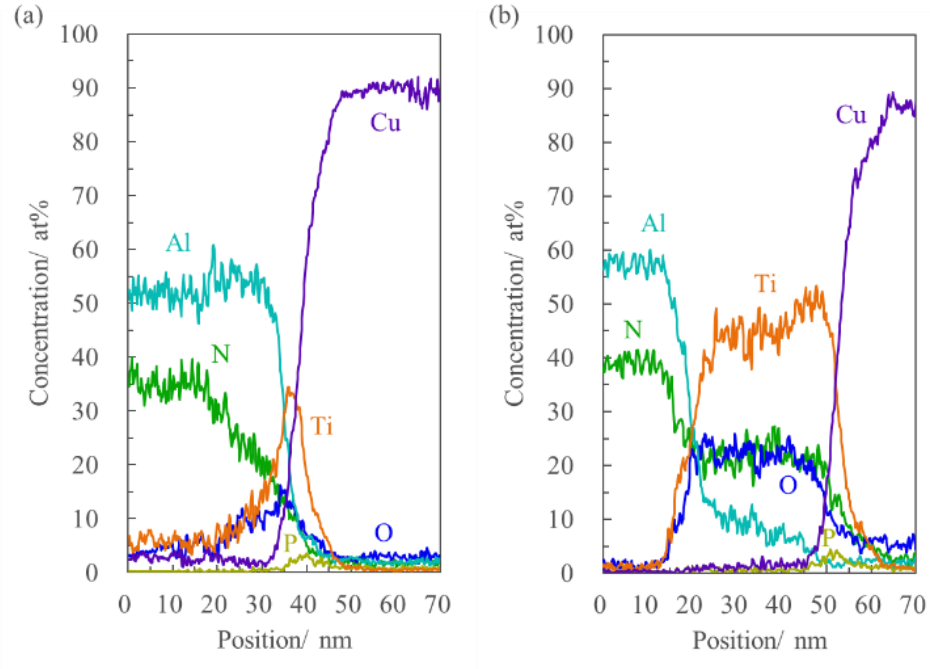

Fig. 5　EDS analyses of a Cu/AlN interfacial reaction layer after bonding for 1 hr with an initial 1 μm thick Ti film at (a) 850 °C and (b) 950 °C. These EDS line profiles were acquired from the lines defined by the yellow arrows shown in the corresponding TEM images in Figs. 4(c) and 4(d), respectively.

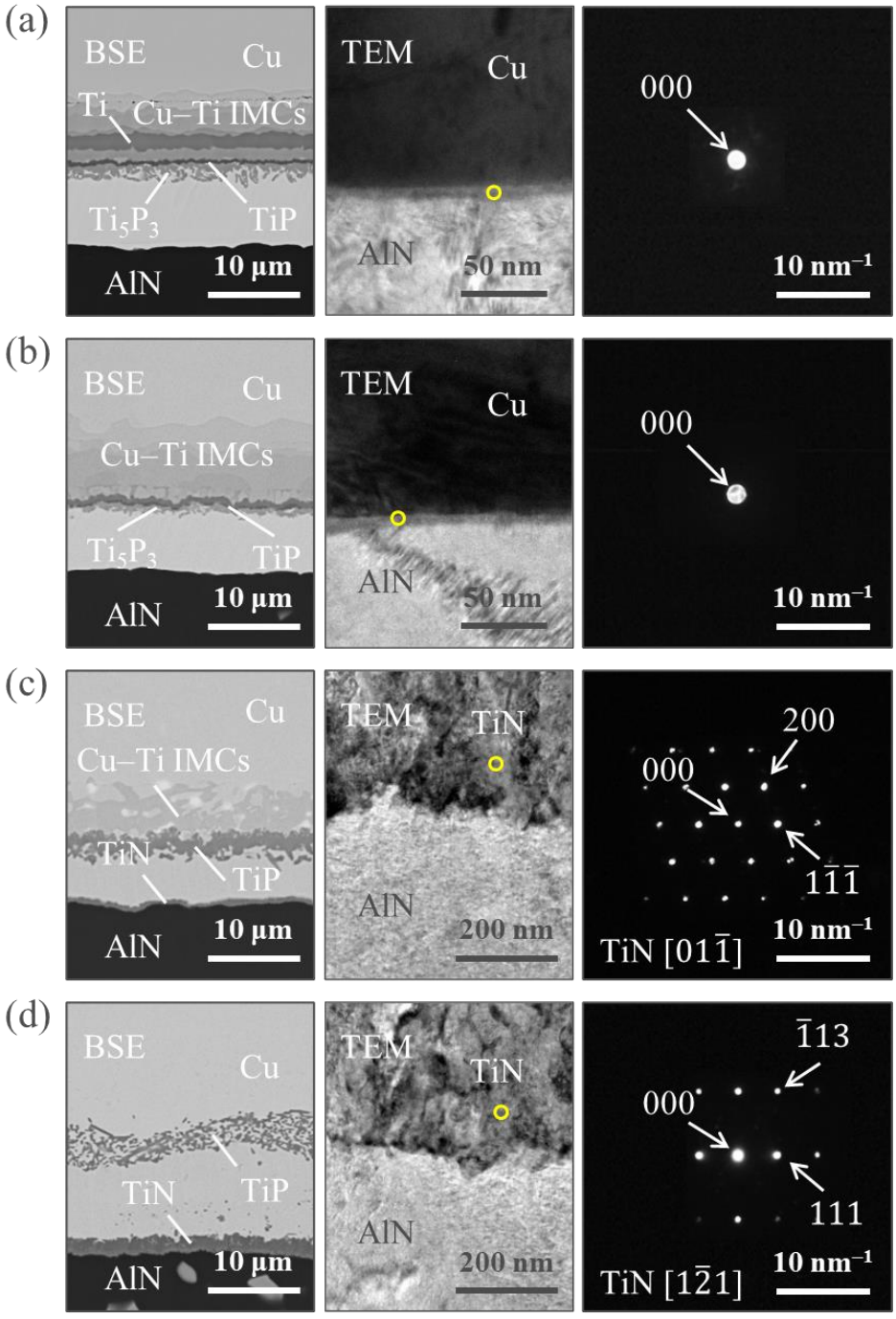

Fig. 6 Cross-sectional BSE and TEM images of a Cu/AlN interface with nano beam electron diffraction patterns of the interfacial reaction layer after bonding for 1 hr with an initial 5 μm Ti foil at (a) 650 °C, (b) 750 °C, (c) 850 °C and (d) 950 °C.

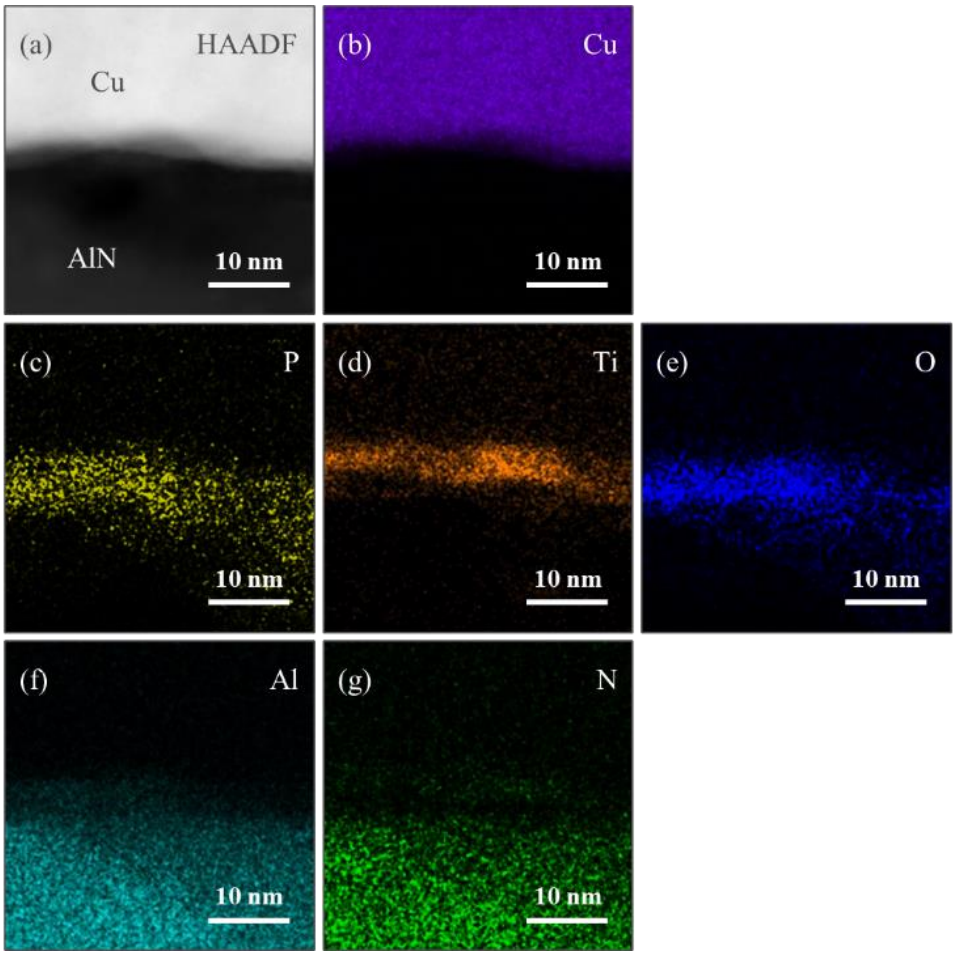

Fig. 7 (a) HAADF image of a Cu/AlN interface after bonding at 650 °C for 1 hr with an initial 5 μm Ti foil, together with the elemental distribution of (b) Cu, (c) P, (d) Ti, (e) O, (f) Al and (g) N obtained by EDS.

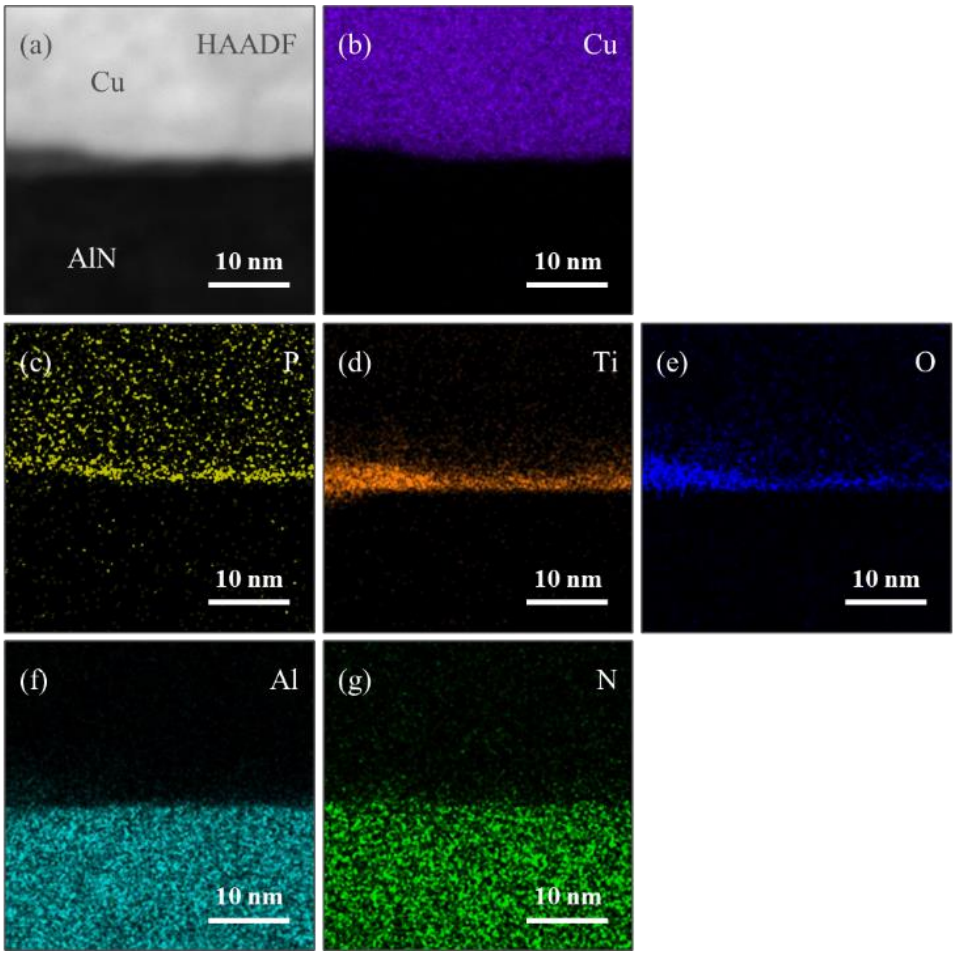

Fig. 8　(a) HAADF image of a Cu/AlN interface after bonding at 750 °C for 1 hr with an initial 5 μm Ti foil, together with the elemental distribution of (b) Cu, (c) P, (d) Ti, (e) O, (f) Al and (g) N obtained by EDS.

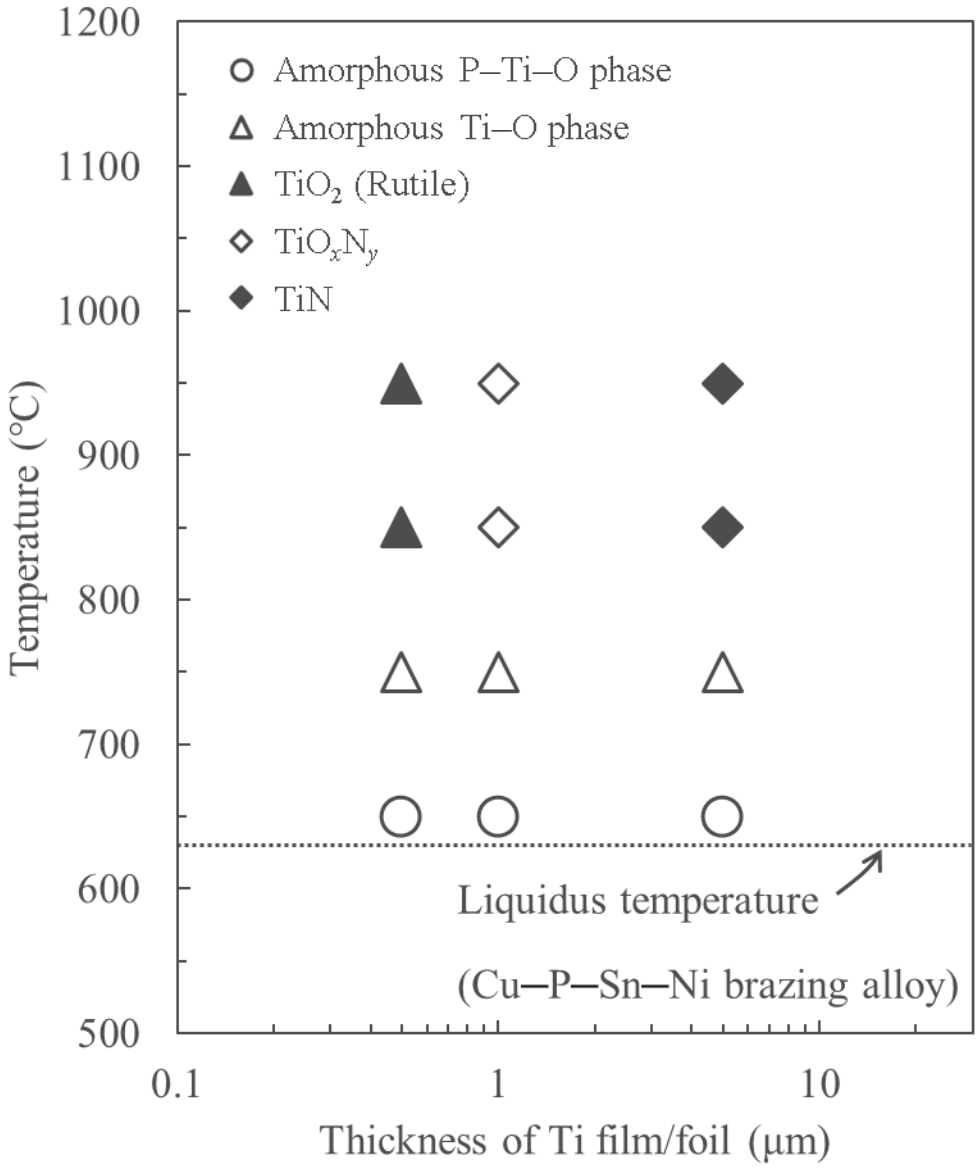

Fig. 9 Cu/AlN interfacial structure classification as a function of temperature and Ti film/foil. thickness.

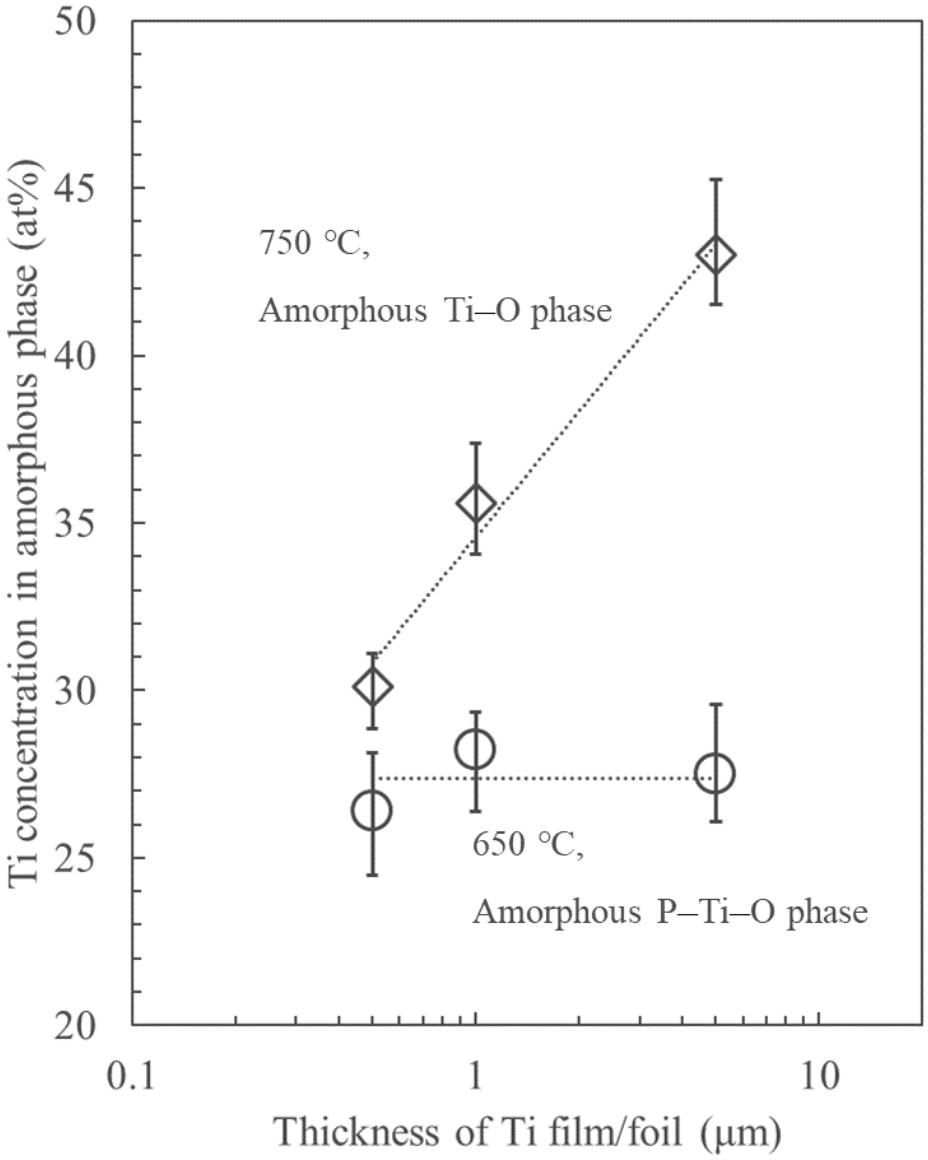

Fig. 10 Dependence of the Ti concentration in the amorphous phase of a Cu/AlN interface on the initial Ti film/foil thickness after bonding for 1 hr at 650 °C and 750 °C. Within experimental error in the 0.5 – 5 μm thickness range shown, the Ti concentration of the amorphous P–Ti–O phase is independent of the initial thickness of the Ti material, whereas that of the amorphous Ti–O phase increases as the initial thickness of the Ti material increases.

Thickness of Ti film/foil	Temperature	Concentration (at%)				
		Cu	P	Sn	Ni	Ti
1 μm	650 ℃	95.6	0.4	3.8	0.2	0.1
	750 ℃	97.8	0.0	1.9	0.2	0.1
5 μm	650 ℃	92.8	0.5	6.1	0.2	0.4
	750 ℃	93.7	0.0	5.8	0.1	0.4

Table 1　Quantitative analysis of a Cu phase 4 μm away from a Cu/AlN bonding interface after bonding for 1 hr at the specified temperatures.